Complex-coefficient systems in control

Troeng, Olof; Bernhardsson, Bo; Rivetta, Claudio

Published in:
Proceedings of the 2017 American Control Conference (ACC)

DOI:
10.23919/ACC.2017.7963201

2017

Document Version:
Peer reviewed version (aka post-print)

Complex-Coefficient Systems in Control

Olof Troeng, Bo Bernhardsson, Claudio Rivetta

***Abstract*— Complex-valued dynamics can be used for modeling rotationally invariant two-input two-output systems and bandpass systems when they are considered in the baseband. In a few instances, control design has been done in the complex domain, which facilitated analysis and synthesis. While previous work has been application specific, we will discuss more generally how complex valued dynamics arise, basic properties of these systems, revisit some classic control theoretic results in the complex setting, and discuss two novel examples of control design in the complex domain — accelerator cavity field control and feedback linearization of RF amplifiers.**

I. Introduction

Certain systems are most conveniently modeled by complex-coefficient differential equations [1]–[10]. In two cases, also control design has been done in the complex domain: regulation of electric machines [1]–[3] and active vibration damping of rotating machinery [4], [5]. For these applications it was found that the complex formulation facilitated design and analysis compared to previous real-valued formulations.

The utility of complex-coefficient representations has also become apparent in the authors' work on accelerator cavity field control at the European Spallation Source [11] and the SLAC National Accelerator Laboratory [12]. When complex-coefficient transfer functions are analyzed in existing cavity field control literature, either the coefficients are assumed to be real, or an equivalent, real-coefficient, two-input two-output representation is considered, which complicates analysis and synthesis. With complex-coefficient systems, the standard Nyquist criterion can be used, rather than the less intuitive MIMO Nyquist criterion as in [14, p. 85].

As remarked in [3], little has been written on complex-coefficient systems in the control literature, some noteworthy examples are: linear systems theory [15], Routh-Hurwitz's stability criterion [16], Kharitonov's theorem [17], the Nyquist stability criterion [18] and root locus [3].

In the next section we look at how complex-coefficient dynamics arise in real-world applications, in Section III we discuss basic properties of complex systems, in Sections IV and V we consider some classic control theoretic results in the complex setting, and in the final two sections we discuss two novel applications of complex-coefficient systems for control analysis: cavity field control and Cartesian feedback linearization of RF amplifiers. In the Appendix we mention some pitfalls when analyzing complex systems with MATLAB.

Olof Troeng and Bo Bernhardsson are with the Department of Automatic Control, Lund University, 22100 Lund, Sweden. They work with developing the RF control system for the linac at the European Spallation Source. Email: {oloft, bob}@control.lth.se Claudio Rivetta is with SLAC National Accelerator Laboratory, Stanford University, CA 94395. Email: rivetta@slac.stanford.edu

The two first authors are members of the ELLIIT Excellence Center. Their work is also supported by the Swedish Research Council through the LCCC Linnaeus Center. C.R. is a member of GISMo, SLAC National Accelerator Laboratory, Stanford University, USA. His work is supported by US Department of Energy, Contract No. DE-AC02-76SF00515.

II. Origin of Complex-Valued Dynamics

A. Rotationally Invariant TITO Systems

A two-input two-output (TITO) system

$$\mathbf{G}(s) = \begin{bmatrix} G_1(s) & -G_2(s) \\ G_2(s) & G_1(s) \end{bmatrix} \tag{1}$$

acting on signals $\begin{bmatrix} x_1 & x_2 \end{bmatrix}^T$ can be compactly represented by the complex SISO system

$$G(s) = G_1(s) + iG_2(s) \tag{2}$$

acting on signals $x_1 + ix_2$.

For example, the dynamics of the Foucault pendulum in the xy-plane, can, subject to small angle approximation, be represented by the complex differential equation

$$\ddot{z} + 2i\Omega\dot{z}\sin\phi + \omega^2 z = 0$$

where $z = x + iy$, ω is the natural frequency of the pendulum, Ω the rotational frequency of the Earth and ϕ is the latitude where the pendulum is located. See [6] for similar examples.

Two other examples are the dynamics of balanced three-phase electric machines, which take the form (1) after application of an $\alpha\beta$-transformation [1]–[3], and vibrations in rotating machines [4], where the states x_1 and x_2 correspond to the x- and y-positions of the rotating shaft.

B. Bandpass Systems

In applications such as telecommunications, where the signals of interest are narrowband around some frequency ω_c, it is convenient to consider the complex envelopes of the signals [7], [19], [20].

If the physical signal is given by

$$\begin{aligned} x_{\mathrm{c}}(t) &= A(t)\cos\left(\omega_c t + \phi(t)\right) \\ &= \mathrm{Re}\left\{A(t)\mathrm{e}^{i\phi(t)}\mathrm{e}^{i\omega_c t}\right\}, \end{aligned} \tag{3}$$

where the modulation, i.e. $A(t)$ and $\phi(t)$, varies slowly, then the complex envelope, or the equivalent baseband signal, is given by

$$\begin{aligned} \mathbf{x}_{\mathrm{BB}}(t) &:= A(t)\mathrm{e}^{i\phi(t)} \\ &= x_{\mathrm{Re}}(t) + ix_{\mathrm{Im}}(t), \end{aligned} \tag{4}$$

where $x_{\mathrm{Re}}(t)$ and $x_{\mathrm{Im}}(t)$ are real-valued.

An input-output-relation

$$Y_c(s) = G_c(s)U_c(s)$$

in the Laplace domain, is conveniently transformed to the base-band via the transformation $s \mapsto s + i\omega_c$, which gives

$$Y_c(s + i\omega_c) = G_c(s + i\omega_c)U_c(s + i\omega_c).$$

$Y_c(s + i\omega_c)$ and $U_c(s + i\omega_c)$ are equivalent baseband signals and thus the equivalent baseband model of $G_c(s)$ can be identified as

$$G_{\text{BB}}(s) = G_c(s + i\omega_c). \tag{5}$$

If the signals of interest are have narrow support around ω_{RF}, high frequency dynamics of $G_{\text{BB}}(i\omega)$ can be neglected. Typically the resulting $G_{\text{BB}}(s)$ has complex coefficients [7].

Example, Baseband model of complex pole pair: The second order resonant system

$$\frac{2\zeta_0\omega_0 s}{s^2 + 2\zeta_0\omega_0 s + \omega_0^2}$$

has a baseband model given by

$$\frac{2\zeta_0\omega_0(s + i\omega_c)}{(s + \zeta\omega_0 + i\omega_0 + i\omega_c)(s + \zeta\omega_0 - i\omega_0 + i\omega_c)}.$$

If $\omega_0 \approx \omega_c$ and the damping factor ζ is small, then for small s the first term in the denominator is $\approx 2i\omega_c$ and the following first-order approximation holds,

$$G_{\text{BB}}(s) \approx \frac{\zeta_0\omega_0}{s + \zeta\omega_0 + i(\omega_c - \omega_0)}.$$

Example, Baseband model of time-delay: The baseband model of a time delay e^{-sT} is $\mathrm{e}^{-(s+i\omega_c)T} = \mathrm{e}^{-sT}\mathrm{e}^{-i\omega_c T}$. If ω_c is large, the phase of baseband model is sensitive to variations in T.

C. Quantum Systems

Linear stochastic quantum systems are naturally described by complex, quantum stochastic differential equations — see [8]–[10] for control design for these systems.

III. Complex Signals and Systems

In the previous section we motivated the study of systems of the form

$$\begin{aligned} \dot{x}(t) &= Ax(t) + Bu(t) \\ y(t) &= Cx(t) + Du(t) \end{aligned} \tag{6}$$

where the signals and matrices are complex. The complex setting gives rise to some peculiarities not seen for real systems. In Fig. 1 it is seen that a first-order complex system may exhibit an oscillatory step response and in Fig. 2 it is seen that the frequency response is not necessarily conjugate symmetric with respect to positive and negative frequencies.

To better understand the structure of the system (6) we split its impulse response into its real and imaginary parts

$$g(t) = g_{\text{Re}}(t) + ig_{\text{Im}}(t).$$

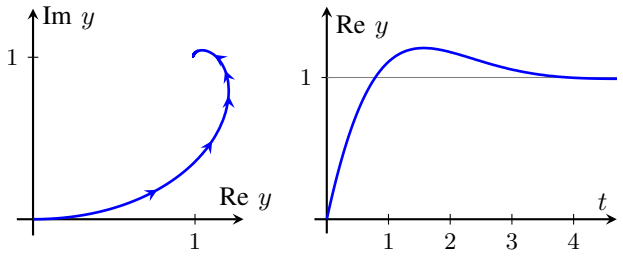

(a) $y(t)$ in $\mathbb{C}$. (b) $\operatorname{Re} y(t)$.

Fig. 1: Step response $y(t)$ of first-order system $2/(s+1-i)$.

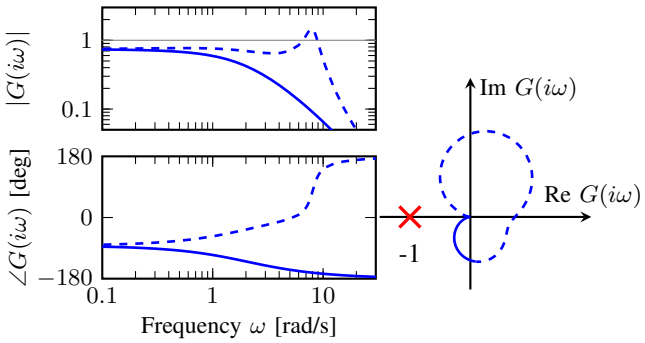

(a) Bode plot. (b) Nyquist curve.

Fig. 2: Frequency response of $G(s) = 12/(s+1+8i)/(s+2)$. Solid lines correspond to $\omega > 0$ and dashed lines to $\omega < 0$.

Denoting the Laplace transform of g_{Re} and g_{Im} by $G_{\text{Re}}(s)$ and $G_{\text{Im}}(s)$ respectively, it is seen that the transfer function for (6) is given by

$$G(s) = G_{\text{Re}}(s) + iG_{\text{Im}}(s). \tag{7}$$

Note that $G_{\text{Re}}(s)$ and $G_{\text{Im}}(s)$ are not the real and imaginary parts of $G(s)$, but that the subscripts are motivated by their relative contribution to the impulse response. Since $g_{\text{Re}}(t)$ and $g_{\text{Im}}(t)$ are real it follows that $g^*(t) = g_{\text{Re}}(t) - ig_{\text{Im}}(t)$ and

$$G^*(\bar{s}) = G_{\text{Re}}(s) - iG_{\text{Im}}(s),$$

due to conjugate symmetry of $G_{\text{Re}}(s)$ and $G_{\text{Im}}(s)$. Thus the decomposition (7) can be recovered from $G(s)$ via

$$G_{\text{Re}}(s) = \frac{G(s) + G^*(\bar{s})}{2}, \quad G_{\text{Im}}(s) = \frac{G(s) - G^*(\bar{s})}{2i}. \tag{8}$$

The action of the complex coefficient transfer function (7) on a signal $x(t) = x_{\text{Re}}(t) + ix_{\text{Im}}(t)$ is illustrated in Fig. 3.

A. Correspondence to Real-Valued Representation

In some applications, [14], [21], the complex transfer function (7) is represented as a real, two-input two-output (TITO) system of the form

$$\mathbf{G}(s) = \begin{bmatrix} G_{\text{Re}}(s) & -G_{\text{Im}}(s) \\ G_{\text{Im}}(s) & G_{\text{Re}}(s) \end{bmatrix}, \tag{9}$$

acting on real-valued vector signals $\begin{bmatrix} x_{\text{Re}} & x_{\text{Im}} \end{bmatrix}^T$.

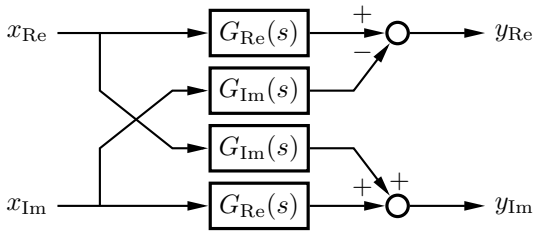

Fig. 3: Illustration of how a complex transfer function $G(s) = G_{\mathrm{Re}}(s) + iG_{\mathrm{Im}}(s)$ acts on a signal $x = x_{\mathrm{Re}} + ix_{\mathrm{Im}}$ to produce a signal $y(t) = y_{\mathrm{Re}} + iy_{\mathrm{Im}}$.

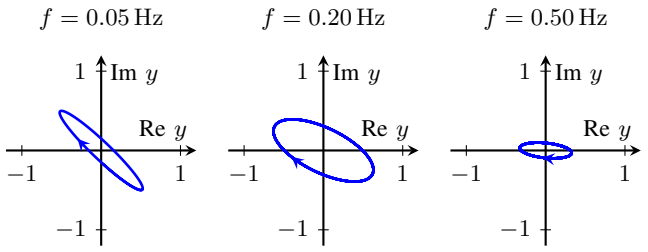

Fig. 4: Lissajous ovals in the complex plane generated by excitation of $1/(s+1+i)$ by $u = \sin(2\pi f t)$.

To better understand the relationship between the real system representation (9) and the complex representation (7), we consider the eigenvalue factorization of (9),

$$\mathbf{G}(i\omega) = \mathbf{S}^* \begin{bmatrix} G(i\omega) & 0 \\ 0 & G(-i\omega) \end{bmatrix} \mathbf{S}, \quad \mathbf{S} = \frac{1}{\sqrt{2}} \begin{bmatrix} 1 & 1 \\ -i & i \end{bmatrix}, \tag{10}$$

from which we see that the eigenvectors are independent of frequency, and that the eigenvector $\begin{bmatrix} 1 & -i \end{bmatrix}^T \leftrightarrow \begin{bmatrix} \cos\omega t & \sin\omega t \end{bmatrix}^T \leftrightarrow \mathrm{e}^{i\omega t}$, and similarly for $\begin{bmatrix} 1 & i \end{bmatrix}^T$.

While the real-coefficient representation (9) is necessary for physical implementation of complex transfer functions, it contains redundant information, and from (10) we see that the frequency responses of $G(i\omega)$ for positive and negative frequencies are intertwined, complicating analysis.

The eigenvectors of $\mathbf{G}(i\omega)$ are orthogonal, so the singular values of $\mathbf{G}(i\omega)$ are the modulus of the eigenvalues, thus

$$||\mathbf{G}||_\infty = ||G||_\infty \tag{11}$$

$$||\mathbf{G}||_2 = \sqrt{2}\,||G||_2\,. \tag{12}$$

B. Response to Signal with Specific Direction

Even if the dynamics of a system is rotationally invariant, and hence can be represented as a complex SISO system, disturbances may have a specific direction. Consider for example phase noise in radio-frequency applications.

To illustrate the general behavior, consider without loss of generality, the output of (6) when subjected to a purely real signal $u(t) = \cos(\omega t)$,

$$\begin{aligned} y(t) = {} & |G_{\mathrm{Re}}(i\omega)| \cos\left(\omega t + \angle G_{\mathrm{Re}}(i\omega)\right) \\ & + i\,|G_{\mathrm{Im}}(i\omega)| \cos\left(\omega t + \angle G_{\mathrm{Im}}(i\omega)\right). \end{aligned} \tag{13}$$

The signal (13) corresponds to Lissajous ovals in the complex plane, see Fig. 4.

IV. Frequency Domain Analysis

When analyzing complex systems in the frequency domain it is necessary to consider both positive and negative frequencies, as illustrated in Fig. 2. For example a factor $\mathrm{e}^{i\epsilon}$ gives the impression of an improved phase margin if only positive frequencies are considered.

A. Nyquist's Stability Criterion

The assumptions and standard proof of the Nyquist stability criterion require no change as the argument principle is valid for any meromorphic function [18].

B. Bode's Sensitivity Integral

Bode's sensitivity integral is typically considered over only positive frequencies [22], however double-sided integration is necessary for complex coefficient transfer functions,

$$\int_{-\infty}^{\infty} \log|S(i\omega)|\,\mathrm{d}\omega = 2\pi \sum_{k=1}^{N_p} \mathrm{Re}\,p_k, \tag{14}$$

where $\{p_k\}$ are the RHP poles of G. Also, unlike the real case, it is crucial to take the real part of the poles in (14). The proof is the same [22].

That the single-sided version of (14) fails to hold in the complex case, is seen from that $G(s + i\delta)$ would correspond to different lower limits of integration for different δ.

C. Bode's Complementary Sensitivity Integral

The relationship for the complementary sensitivity function [23] needs the same modifications as in (14) to cover complex coefficient transfer functions,

$$\int_{-\infty}^{\infty} \log|T(i\omega)|\,\frac{\mathrm{d}\omega}{\omega^2} = -\pi K_v^{-1} + \pi\tau + 2\pi \sum_{k=1}^{N_z} \mathrm{Re}\frac{1}{z_k}, \tag{15}$$

where τ is the system time-delay, $\{z_k\}$ are the RHP zeros of $G(s)$ and $K_v = \lim_{s\to 0} sL(s)$. The result follows, with minor modifications, from the proof in [23].

D. Bode's Gain-Phase Relationship

Bode's gain-phase relationship which relates the phase of a real, minimum phase system $G(s)$, to the slope of its gain curve in logarithmic scale, does not hold for complex $G(s)$. The less intuitive relationship given by the double-sided version of the Kramers-Kronig relations [24],

$$\angle G(i\omega_0) = \frac{1}{\pi}\mathcal{P}\int_{-\infty}^{\infty} \frac{\log|G(i\omega)|}{\omega - \omega_0}\,\mathrm{d}\omega,$$

where $\mathcal{P}$ denotes the Cauchy principle value, still holds for complex, minimum phase systems.

V. State-space Analysis

Notions such as controllability, stability, etc. are analogous to the real case [15]. Below, some special results are discussed in more detail.

A. $\mathcal{H}_2$ and $\mathcal{H}_\infty$ Norms

The H_2-norm can be calculated using the same formulas as in the real case, i.e. $\|C(sI-A)^{-1}B\|_2^2 = \text{trace}\,(B^*YB) = \text{trace}\,(CXC^*)$, where $X = X^*$ and $Y = Y^*$ are solutions to the complex Lyapunov equations $XA + A^*X + B^*B = 0$ and $AY + YA^* + CC^* = 0$ respectively.

The linear matrix inequalities for calculating the H_∞-norm also carry over, given that Hermitian transposition is used.

Remark: MATLAB's functions for $\mathcal{H}_\infty$-synthesis does not handle complex systems correctly.

B. LQR

In [15] the optimal feedback for a complex linear system with respect to a cost functional

$$J = \int_0^\infty \begin{bmatrix} x(t) & u(t) \end{bmatrix}^* \begin{bmatrix} Q & N \\ N^* & R \end{bmatrix} \begin{bmatrix} x(t) \\ u(t) \end{bmatrix} \mathrm{d}t$$

is derived. The optimal feedback is given by $u = -Kx$ with

$$K = R^{-1}(N^* + B^*X),$$

where the Hermitian matrix $X \geq 0$ satisfies the complex Riccati equation

$$A^*X + X^*A - (N + XB)R^{-1}(N^* + B^*X) + Q = 0.$$

For a first order system it seen that when $N = 0$, BK is real and positive, and the linear optimal regulator moves the closed loop pole, $A - BK$, parallel to the real axis, further into the LHP.

The amazing robustness properties of LQR (for $N = 0$), that hold in the real case (infinite gain margin and $\geq 60^\circ$ phase margin), hold also in the complex case, even if the Nyquist curve is not symmetric with respect to the real axis.

C. Kalman Filter for Complex-Valued Normally Distributed Noise

It is natural to allow the state and measurement noise to be complex-valued. A complex-valued normally distributed variable Z with zero mean is determined by the matrices $E(ZZ^*)$ and $E(ZZ^T)$. If the latter is zero, one says that Z is circular-symmetric, which means that the distribution function is rotationally invariant in the complex plane. The paper [25] discusses the general problem and introduces the concept of "widely linear state space models" to describe the optimal estimator in an aesthetic form.

VI. Example I: Amplifier Linearization

Cartesian feedback linearization of power amplifiers was actively studied 10–20 years ago as a means to reduce power consumption and adjacent channel interference in telecommunications [26]–[28]. To avoid instability and performance degradation, the phase shift ϕ between up- and down-conversion needs to be properly compensated by an adjustment phase $\hat{\phi}$, see Fig. 5.

If the amplifier is operating in an almost linear region, the open loop system is well approximated by

$$G(s) = H(s)P(s)\mathrm{e}^{-\tau s}\mathrm{e}^{i\delta}, \tag{16}$$

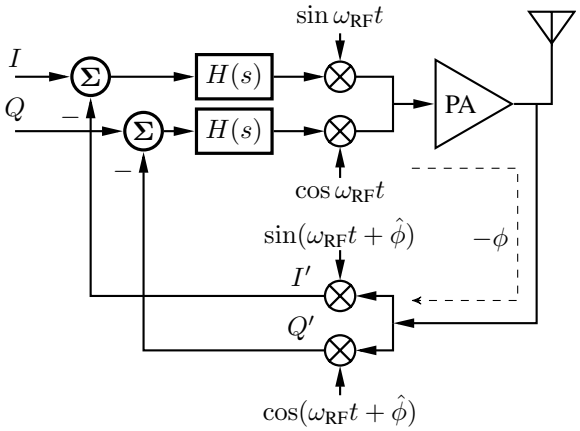

Fig. 5: Amplifier linearization by Cartesian feedback [28], loop filters, up- and down-conversion mixers are shown.

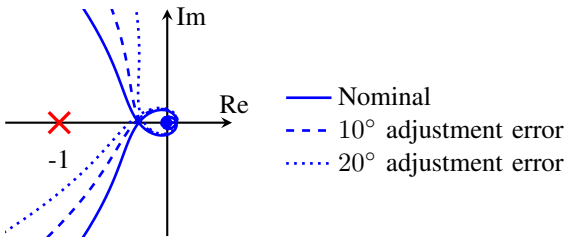

Fig. 6: Nyquist curves for Cartesian feedback loop with different phase adjustment errors. The nominal curve is from [26, Sec. 4.2].

where $H(s)$ is the loop filter, $P(s)$ is a baseband model of the mixer and amplifier dynamics, τ is the loop delay and $\delta := (\hat{\phi} - \phi)$ is the phase adjustment error.

Although [29] simulated (16) as a complex systems, the stability properties were analyzed using the equivalent TITO form (1). After algebraic computations and a clever observation it was shown that an adjustment error δ translates directly to a corresponding reduction in phase margin.

In the complex setting the same conclusion follows directly from the Nyquist criterion (Sec. IV-A), by noting that the factor $\mathrm{e}^{i\delta}$ corresponds to a rotation of the Nyquist curve $H(i\omega)P(i\omega)\mathrm{e}^{-i\tau\omega}$ by δ radians, see Fig. 6 for an illustration.

VII. Example II: Cavity Field Control

In radio-frequency accelerators, particle bunches are accelerated by electromagnetic fields confined in RF cavities. The amplitude of the fields, and their phase relative the particle bunches, need to be precisely controlled [30].

To see how complex transfer functions play a role in this, we first derive the baseband equations for the cavity and the RF system (Fig. 7), and then design a complex $\mathcal{H}_\infty$-controller.

A. Model of Cavity Dynamics

From Maxwell's equations it follows that the electric field in the cavity can be expressed as a linear combination of

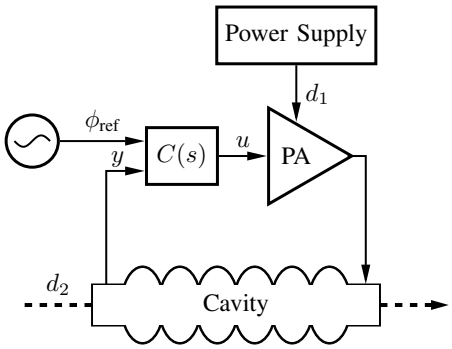

Fig. 7: Block diagram of RF system for one cavity. Variations in the voltage supply to the power amplifier (d_1) and ripple on the accelerated current (d_2), affect the system as load disturbances on the cavity input.

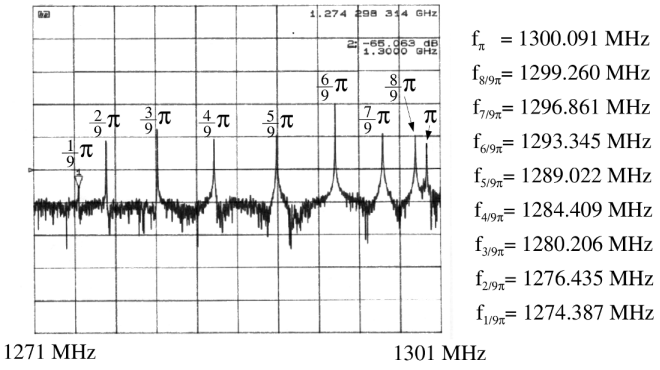

Fig. 8: Fundamental passband modes in the nine-cell TESLA cavity [14], that is used in many large accelerators, e.g. LCLS II. The π-mode is used for particle acceleration, while all other modes are detrimental to both particle acceleration and RF system stability.

eigenmodes,

$$\mathcal{E}(r,t) = \sum_{k=0}^{\infty} v_k(t)\mathbf{E}_k(r),$$

where the mode amplitudes e_k satisfy [30, Ch 5, 10]

$$\frac{d^2}{dt^2}v_k + 2\gamma_k\frac{d}{dt}v_k + \omega_k^2 v_k = 2\kappa_k\frac{d}{dt}i_g + 2\alpha_k\frac{d}{dt}i_b, \quad (17)$$

where ω_k is the resonance frequency and γ_k the half bandwidth of mode k. κ_k and α_k quantify how the output of the power amplifier, modeled as a current i_g, and the accelerated particle current i_b, couple to the cavity field. The amplifier output i_g, can considered as the control signal. Variations in i_b enter as load disturbances.

The distribution of modes in the fundamental passband for an elliptical cavity is shown in Fig. 8. The mode that is used for particle acceleration is typically the π-mode, and the purpose of the RF system is to excite the π-mode and control its phase and amplitude.

After both Laplace and baseband transformations of (17), we get

$$V_k(s) := \frac{1}{s+\gamma_k+i\Delta\omega_k}\left(\kappa_k I_g(s) + \alpha_k I_b(s)\right), \quad (18)$$

where $\Delta\omega_k = \omega_{\text{RF}} - \omega_k$.

A baseband model of the RF system in Fig. 7, including the accelerating π-mode and one parasitic mode, now takes the form

$$P(s) = P_{\text{amp}}(s)\mathrm{e}^{-i\omega_{\text{RF}}\tau}\mathrm{e}^{-\tau s} \times \left[\frac{c_\pi\kappa_\pi/2}{s+\gamma_\pi+i\Delta\omega_\pi} + \frac{c_1\kappa_1/2}{s+\gamma_1+i\Delta\omega_1}\right], \quad (19)$$

where $P_{\text{amp}}(s)$ is the dynamics of the power amplifier, τ is the system time delay, c_k quantify the coupling of mode k to the measurement probe, and $\mathrm{e}^{-i\omega_{\text{RF}}\tau}$ is an additional factor resulting from the baseband transformation of the loop delay (cf. II-B). Complex quantities in (19) have been highlighted.

B. $\mathcal{H}_\infty$-synthesis Example

As we demonstrate in the Appendix, the MATLAB functions for $\mathcal{H}_\infty$-synthesis does not work for complex coefficient systems, instead we used the TITO representation (1), which resulted in a controller that also had structure (1), from which we recovered a complex controller.

1) Specifications: The main requirements for cavity field control is to suppress load disturbances while maintaining good robustness and avoiding excessive control signal activity. These requirements correspond to the following weights for mixed sensitivity synthesis,

$$\begin{aligned} W_S(s) &= 1 \\ W_{PS}(s) &= k_1 \cdot \frac{1}{s+\epsilon} \\ W_{KS}(s) &= k_2 \cdot \frac{s+\omega_{\text{bw}}}{s+N\omega_{\text{bw}}}. \end{aligned}$$

By tuning how the parameters of the weighting functions, we arrived at a reasonable controller design.

2) Results: The frequency response of the controller is shown in Fig. 9, note the asymmetry with respect to positive and negative frequencies, which imply that the controller has complex-coefficients. It can also be seen that a notch has been by the $\mathcal{H}_\infty$-design, which allow a high control bandwidth for negative frequencies, without introducing positive feedback via the parasitic mode. The gang of four for the design is shown in Fig. 10.

VIII. Conclusions

We have described some applications where system dynamics are conveniently modeled by complex-coefficient systems. Most control theoretic results developed for the real-valued case carry to the complex setting with minor changes, such as ensuring that transposition is Hermitian and that both negative and positive frequencies are considered. Instances where complex systems are erroneously handled by MATLAB were pointed out.

A design example for cavity field control was presented in some detail and it was demonstrated that it was possible to synthesize a complex $\mathcal{H}_\infty$ controller. Due to the special structure of the plant, with resonance peaks only occurring at negative frequencies, the optimal controller had a markedly

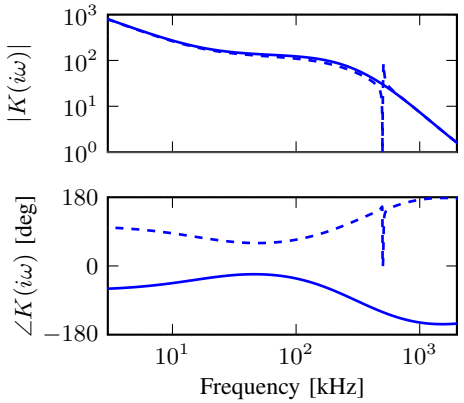

Fig. 9: Bode plot of $\mathcal{H}_\infty$-controller K, solid (dashed) lines correspond to positive (negative) frequencies.

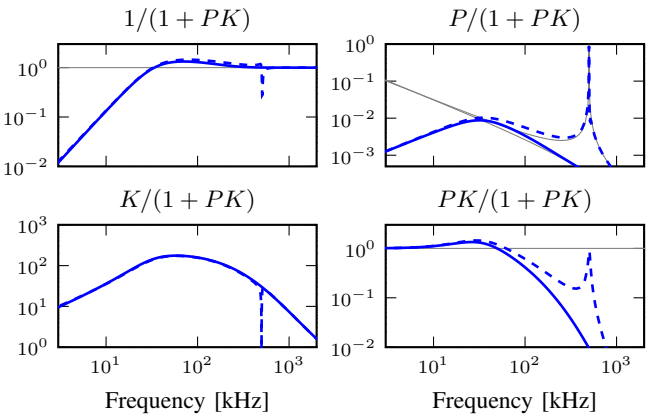

Fig. 10: Gang of four for the $\mathcal{H}_\infty$-design. The frequency response is not conjugate symmetric, so both positive frequencies (solid) and negative frequencies (dashed) are shown. The gray curves in the upper right plot is the frequency response of the plant P.

different frequency response for positive and negative frequencies.

We believe that there are many applications where a complex approach could bring increased insight and that there are related control theoretical questions worthy of further investigation.

References

[1] D. W. Novotny and J. H. Wouterse, "Induction machine transfer functions and dynamic response by means of complex time variables", *IEEE Trans. Power App. Syst.*, vol. 95, no. 4, pp. 1325–1335, Jul. 1976.

[2] L. Harnefors, "Modeling of three-phase dynamic systems using complex transfer functions and transfer matrices", *IEEE Trans. Ind. Electron.*, vol. 54, no. 4, pp. 2239–2248, Aug. 2007.

[3] A. Dòria-Cerezo and M. Bodson, "Design of controllers for electrical power systems using a complex root locus method", *IEEE Trans. Ind. Electron.*, vol. 63, no. 6, pp. 3706–3716, Jun. 2016.

[4] S.-W. Byun and C.-W. Lee, "Pole assignment in rotating disk vibration control using complex modal state feedback", *Mech. Syst. and Signal Process.*, vol. 2, no. 3, pp. 225–241, 1988.

[5] Y. Ren, D. Su, and J. Fang, "Whirling modes stability criterion for a magnetically suspended flywheel rotor with significant gyroscopic effects and bending modes", *IEEE Trans. Power Electron.*, vol. 28, no. 12, pp. 5890–5901, Dec. 2013.

[6] A. B. Pippard, *The Physics of Vibration*. New York, NY: Cambridge University Press, 2007.

[7] K. W. Martin, "Complex signal processing is not complex", *IEEE Trans. Circuits Syst. I, Reg. Papers*, vol. 51, no. 9, pp. 1823–1836, Sep. 2004.

[8] K. Beauchard, J. M. Coron, M. Mirrahimi, and P. Rouchon, "Implicit Lyapunov control of finite dimensional Schrödinger equations", *Syst. & Control Lett.*, vol. 56, no. 5, pp. 388–395, 2007.

[9] M. R. James and R. L. Kosut, "Quantum estimation and control", in *The Control Systems Handbook: Control System Applications*, W. S. Levine, Ed., 2010, ch. 31.

[10] D. Dong and I. R. Petersen, "Quantum control theory and applications: A survey", *IET Control Theory & Applicat.*, vol. 4, no. 12, pp. 2651–2671, 2010.

[11] S. Peggs *et al.*, "ESS technical design report", Tech. Rep. ESS-doc-274, 2013.

[12] J. Arthur *et al.*, "Linac coherent light source (LCLS) II, conceptual design report", Stanford Linear Accelerator, Tech. Rep. SLAC-R-593, 2002.

[13] S. Pfeiffer, "Symmetric grey box identification and distributed beam-based controller design for free-electron lasers", PhD thesis, Technische Universität Hamburg-Harburg, 2014.

[14] T. Schilcher, "Vector sum control of pulsed accelerating fields in Lorentz force detuned superconducting cavities", PhD thesis, Hamburg University, 1998.

[15] P. Lancaster and L. Rodman, *Algebraic Riccati Equations*. Oxford, UK: Oxford University Press, 1995.

[16] E. Frank, "On the zeros of polynomials with complex coefficients", *Bulletin of the Amer. Math. Soc.*, vol. 52, no. 2, pp. 144–157, 1946.

[17] N. Bose and Y. Shi, "A simple general proof of Kharitonov's generalized stability criterion", *IEEE Trans. Circuits Syst.*, vol. 34, no. 10, pp. 1233–1237, Oct. 1987.

[18] S. Gataric and N. R. Garrigan, "Modeling and design of three-phase systems using complex transfer functions", in *30th Annu. IEEE Power Electron. Specialists Conf.*, vol. 2, 1999, pp. 691–697.

[19] R. E. Crochiere and L. R. Rabiner, *Multirate Digital Signal Pocessing*. Englewood Cliffs, NJ: Prentice Hall, 1983.

[20] P. J. Schreier and L. L. Scharf, *Statistical Signal Processing of Complex-Valued Data: The Theory of Improper and Noncircular Signals*. Cambridge, UK: Cambridge University Press, 2010.

[21] J. L. Dawson and T. H. Lee, "Cartesian feedback for RF power amplifier linearization", in *Proc. 2004 Amer. Control Conf.*, vol. 1, Jun. 2004, pp. 361–366.

[22] J. S. Freudenberg and D. P. Looze, "Right half plane poles and zeros and design trade-offs in feedback systems", *IEEE Autom. Control*, vol. 30, no. 6, pp. 555–565, 1985.

[23] R. Middleton and G. Goodwin, *Digital Control and Estimation: A Unified Approach*. Englewood Cliffs, NJ: Prentice Hall, 1990, pp. 423–433.

[24] R. Kronig, "On the theory of dispersion of X-rays", *J. Opt. Soc. Am.*, vol. 12, no. 6, pp. 547–557, 1926.

[25] D. H. Dini and D. P. Mandic, "Class of widely linear complex Kalman filters", *IEEE Trans. Neural Netw.*, vol. 23, no. 5, pp. 775–786, May 2012.

[26] M. Johansson, "Linearization of RF power amplifiers using cartesian feedback", Lic. thesis, Lund University, 1991.

[27] M. A. Briffa and M. Faulkner, "Stability analysis of Cartesian feedback linearisation for amplifiers with weak nonlinearities", *IEE Proceedings - Communications*, vol. 143, no. 4, pp. 212–218, Aug. 1996.

[28] J. L. Dawson, "Feedback linearization of RF power amplifiers", PhD thesis, Stanford University, 2003.

[29] M. A. Briffa, "Linearization of RF power amplifiers", PhD thesis, Victoria University of Technology, 1996.

[30] T. P. Wangler, *RF Linear Accelerators*, 2nd ed. Weinheim, Germany: Wiley-VCH, 2008.

APPENDIX

MATLAB handles complex-coefficient systems incorrectly. We detected the following issues with version R2016a (Linux).

In the `nyquist` plot, the frequency response for negative frequencies equals that at positive frequencies, which is incorrect for complex coefficients system. `hinfnorm` only considers positive frequencies, while `minreal` does not support complex data at all.

The first example of $\mathcal{H}_\infty$-synthesis in the MATLAB documentation,

```
G = (s-1)/(s+1)^2;
W1 = 0.1*(s+100)/(100*s+1);
W2 = 0.1;
[~,~,GAM] = mixsyn(G,W1,W2,[])
```

gives `GAM=0.23`. Multiplying the plant `G` by a complex factor `exp(0.4i)` should not affect the resulting value, as the factor could be canceled by the controller. However the result in this case is `GAM=0.40`, thus demonstrating incorrectness.